The role of adsorbate–adsorbate interactions in the rate controlling step and the most abundant reaction intermediate of NH_3 decomposition on Ru

A.B. Mhadeshwar, J.R. Kitchin, M.A. Barteau, and D.G. Vlachos*

Department of Chemical Engineering, Center for Catalytic Science and Technology, University of Delaware, Newark, DE 19716–3110

Received 14 November 2003; accepted 28 April 2004

N–N adsorbate–adsorbate interactions on a Ru(0001) surface are first estimated using quantum mechanical density functional theory (DFT) calculations, and subsequently incorporated, for the first time, in a detailed microkinetic model for NH_3 decomposition on Ru using the unity bond index-quadratic exponential potential (UBI–QEP) method. DFT simulations indicate that the cross N–H interactions are relatively small. Microkinetic model predictions are compared to ultra-high vacuum temperature programmed desorption and atmospheric fixed bed reactor data. The microkinetic model with N–N interactions captures the experimental features quantitatively. It is shown that the N–N interactions significantly alter the rate determining step, the most abundant reaction intermediate, and the maximum N*-coverage, compared to mechanisms that ignore adsorbate–adsorbate interactions.

KEY WORDS: microkinetic modeling; thermodynamic consistency; rate determining step; most abundant reaction intermediate; adsorbate–adsorbate interactions; density functional theory; ammonia; hydrogen.

1. Introduction

Ammonia synthesis is one of the most extensively studied catalytic processes due to its use in the manufacture of agricultural fertilizers. Ammonia decomposition chemistry, on the other hand, has only recently become of interest due to the desire to produce hydrogen for fuel cells, e.g., see [1] for the application of post microreactors for hydrogen production through ammonia decomposition. Industrially, the prevailing catalyst for ammonia synthesis is reduced Iron (the Haber–Bosch process [2,3]). Ruthenium (Ru) based catalysts have also been studied due to their higher activity at lower H_2/N_2 ratios and lower tendency to poisoning by NH_3 compared to reduced Iron [4,5]. Ru appears to be the best single metal catalyst for NH_3 synthesis and decomposition [6,7] and is the focus of this paper.

Considerable experimental and theoretical research has been devoted to the understanding of NH_3 chemistry on Ru. Temperature programmed desorption (TPD) [8,9], temperature programmed surface reaction (TPSR) [10], temperature programmed adsorption (TPA) [9], laser assisted associative desorption (LAAD) [11,12], molecular beam experiments [4], etc., have provided insights into the underlying physics and the estimation of kinetic parameters. Ultra-high vacuum (UHV) TPA and TPD experiments for the stable species N_2, H_2, and NH_3 can be useful in estimating their adsorption energetics along with those of N and H. Most published models have focused on NH_3 synthesis on Fe. As an example, Dahl *et al.* [13] proposed a rate expression for NH_3 synthesis on Ru assuming N_2 dissociation to be the rate-determining step (RDS). Models, ranging from reduced rate expressions [4,14,15] to detailed elementary-like step mechanisms[10,15], have also been proposed to capture the experimental features on Ru. Given the recent interest in hydrogen production, it is therefore important to develop models that also describe NH_3 decomposition well.

There is a general consensus that N_2 dissociative adsorption is the RDS in NH_3 synthesis from N_2 and H_2 on Ru due to a high activation energy barrier [6,9,11–13,16,17], whereas the N_2 desorption and the N–H bond cleavage have been proposed as the RDS in NH_3 decomposition[4,14]. However, as elaborated below, contradictory evidence is found in the literature regarding the maximum coverage of N* on Ru [4,13,16], and the associated issue of the most abundant reaction intermediate (MARI). Since the MARI can control the coverages of the surface species involved in the RDS of the process [18] along with the apparent reaction orders of reactants, its elucidation is important. In addition, adsorbate–adsorbate interactions can change the MARI and the RDS, an issue that has not been explored in the past for the NH_3 chemistry.

In this paper, first we provide a literature overview of some of the mechanistic aspects of NH_3/Ru chemistry. Then quantum mechanical density functional theory (DFT) calculations on Ru(0001) are presented to

*To whom correspondence should be addressed.
E-mail: vlachos@che.udcl.edu.

1011-372X/04/0700–0013/0 © 2004 Plenum Publishing Corporation

estimate the N–N and N–H interactions. Subsequently, a microkinetic model is developed and parameter optimization is carried out. After performing the simulations, we show how the incorporation of the N–N repulsive adsorbate–adsorbate interactions alters the dominant NH_3 chemistry on Ru. The novelty of this work lies in the inclusion of N–N interactions in microkinetic NH_3/Ru chemistry models that can describe NH_3 decomposition data. Furthermore, we demonstrate that there is not a unique set of parameters that adequately describes the experimental data and that the N–N adsorbate interactions, whose importance was previously underestimated, play a key role in the dominant chemistry.

2. Literature overview of NH_3 chemistry on Ru

While there is a general consensus about the RDS in NH_3 decomposition and synthesis chemistry, some experimental observations are not in line with previously published modeling results. Most research groups have considered N* to be the MARI on Ru. However, for NH_3 decomposition, Tsai and Weinberg [4] proposed that at high temperatures and/or low pressures, empty sites (*) dominate the surface and the cleavage of N–H bond actually controls the rate of the process. Using microkinetic modeling, Dahl *et al.* [16] showed that NH* and H* are the MARI for NH_3 synthesis conditions. In a more recent paper, Dahl *et al.* [13] showed that for one set of operating conditions (inlet NH_3 content = 0.02%), H* is the MARI on Ru, whereas for another set of conditions (inlet NH_3 content = 0.2%), N* is the MARI. Other intermediates, *viz.*, NH* and NH_2* have previously been shown to exist using HREELS experiments[19,20]. These species are strongly adsorbed, but due to lower activation energies for dehydrogenation, they are expected to undergo rapid decomposition to form more stable N-species.

Another mechanistic issue is related to the maximum possible N*-coverage on Ru. Experimentally, stable configurations were observed by Schwegmann *et al.* [21] for a coverage of $\theta_N = 0.25$ and $\theta_N = 0.33$ adlayers using low-energy electron diffraction (LEED). Using a special procedure, Dietrich *et al.* [22] prepared a maximum N*-coverage corresponding to $\theta_N = 0.38$. Rauscher *et al.* [23] observed higher N*-coverages corresponding to $\theta_N = 0.44$. Finally, Diekhoner *et al.* [17] were able to achieve N*-coverages up to 1 ML N/Ru for high N doses, but the higher coverage structures were proposed to be metastable. DFT simulations performed by Jacobi [24] suggested that N*-coverages higher than ~0.7 should be unstable. Eventhough the experimental and DFT evidence suggests that N*-coverages above ~0.7 should be unstable, some modeling results showed N*-coverages close to 1.0, e.g., [4].

Finally, there has been some disagreement about the adsorbate–adsorbate repulsive interactions between N atoms on Ru. The DFT calculations by Jacobi [24], Hammer[25], and Logadottir and Norskov (presented in [17]) clearly showed strong N–N interactions. Mortensen *et al.* [26] suggested that there is a substantial N–N repulsion above quarter monolayer coverage. Consequently, the activation energy and the heat of reaction for associative desorption of N_2 should also be coverage dependent. N_2-TPD data by Dahl *et al.* [8] for different initial N*-coverages shows that the desorption peak shifts towards lower temperatures with increasing coverage more than anticipated from an associative second-order desorption, indicating possible repulsive N–N interactions. Hinrichsen *et al.* [9] also inferred this through their N_2-TPD studies, and on this basis, they implemented coverage dependent activation energy for N_2 adsorption in the TPA modeling. In contrast, Tsai and Weinberg [4] inferred that the desorption activation energy is practically independent of N*-coverage.

Obviously, it is possible that some of the apparent discrepancies in the literature may be due to the different operating conditions and catalysts, ranging from UHV to high pressures (1–50 atm) and from single crystals to supported catalysts to promoted catalysts. A microkinetic model that can describe data over a wide range of conditions, while including adsorbate–adsorbate interactions, is therefore highly desirable to provide further insights into the aforementioned issues.

3. Quantum mechanical DFT calculations

Parameter estimation for real catalysts from DFT simulations is a daunting multiscale problem that has its roots in the well-known materials' gap. Specifically, many reactions, including NH3 synthesis, are known to be structure sensitive. The difference in sticking coefficients or predicted energetics [27,28] is an example of such structure sensitivity. On the other hand, the rate (or sticking coefficient) of dissociative chemisorption of nitrogen has been found experimentally to be equal on different single crystal surfaces, *viz.*, Ru (0001), Ru $(10\bar{1}0)$, and Ru $(11\bar{2}1)$, including small Ru particles on MgO support [9,29,30]. To reconcile these issues, Ertl [30] mentioned that such structural insensitivity is due to slow adsorption of N2 on terrace sites, followed by diffusion to the active step sites and dissociation. Given the multiscale complexity of catalytic processes and compensation of various effects, it is not unusual that a microkinetic model with UHV-based rate parameters, e.g. [31], can be adequate over a wide range of conditions (1–300 atm and 375–500°C), despite the structure sensitivity of a reaction. Our approach follows in a way this premise but we rely as much as possible on experimental heats of chemisorption, which hopefully capture the energetics closer on practical catalysts. Our

primary objective of performing DFT calculations is then to obtain estimates for lateral interactions needed for microkinetic simulations. The possible number of interactions grows very rapidly as the number of surface species increases. In fact our approach is hierarchical in nature as outlined in [32] i.e., after predicting the major species we estimate the relevant interactions and repeat the simulations, and we may have to repeat this process a few times until a self-consistent input/output emerges (see [32] for an example). Here, for simplicity we leave out such iterations.

DFT calculations are carried out on (2×2) repeated surface cells of three layers thick Ru(0001) slabs, with all the three layers being relaxed. A typical picture of Ru(0001) slab along with the N adsorbate is shown in the inset of figure 1. A plane wave basis set with an energy cutoff of 350 eV is employed with 18-k Chadicohen point mesh. The PW91 exchange-correlation functional is applied and the Vanderbilt ultrasoft pseudopotential [33] is used to describe the core electrons. The DACAPO [34] code has been employed for our DFT calculations.

Energies for four different (symmetrically arranged equilibrium positions) N*-coverages ($\theta_N = 0.25$, 0.5, 0.75, and 1.0) are estimated along with the energetics for the zero coverage Ru(0001) slab and the gas phase N-atom. The vertical distance between the N-atom on a hollow site and the Ru layer is 1.17 Å and the Ru–N bond length is 1.99 Å. These values compare well with slab DFT calculations of Schwegmann *et al.* [21] (bond length = 1.94 Å), Jacobi [24] (bond length = 2.00 Å), Zhang *et al.* [35] (layer spacing = 1.09 Å), cluster DFT calculations of Dooling *et al.* [36] (bond length = 1.99 Å), and LEED experimental observations of Schwegmann *et al.* [21] (bond length = 1.93 Å). The N*-adsorption site is threefold hcp hollow, in agreement with the literature [21,24,36]. The energetics for the adsorbates on the slab is shown in figure 1. The heat of nitrogen chemisorption is found to vary linearly with N*-coverage. The coverage-dependent heat of chemisorption (Q_N) is given as $Q_N = 128.2 - 33.3\theta_N$ kcal/mol. The adsorbate–adsorbate interactions of 33.3 kcal/mol/ML are strongly repulsive, and can play an important role in surface chemistry. Our calculations match fairly well with those of Jacobi [24] (36.3 kcal/mol/ML) and Logadottir and Norskov (reported in [17] as 33.9 kcal/mol/ML).

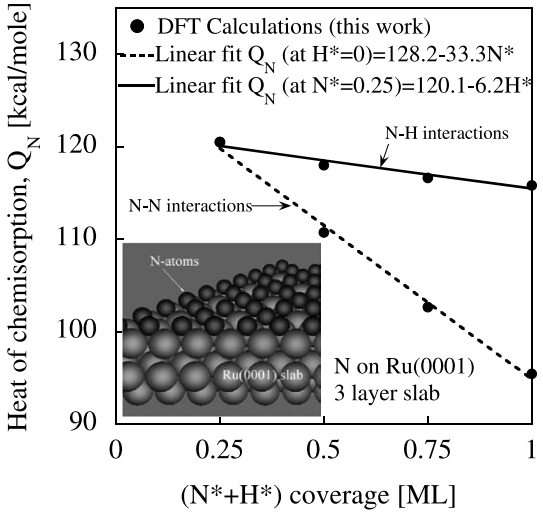

Figure 1. Heat of nitrogen chemisorption versus N*-coverage ($\theta_H = 0$) using DFT calculations on a three-layer Ru(0001) slab. The inset shows the Ru slab with N-atoms, corresponding to an N*-coverage of 0.75 ML. The dotted line is a linear fit to the calculation points. Strong repulsive N–N interactions of 33.3 kcal/mol/ML are found. The solid line is a linear fit of N–H interactions as a function of H* coverage for fixed $\theta_N = 0.25$. N–H interactions of 6.2 kcal/mol/ML are weak compared to the N–N interactions.

Aside from the N–N interactions, we also calculated the heats of chemisorption for H* and NH_x* species, and tabulated them in column 3 of table 1. Zero-point energy corrections are not accounted for in our calculations. As shown below, under typical decomposition conditions, both N* and H* are in significant fractions. Therefore, the cross interactions of N* at 0.25 monolayer (a single N-atom on the 2×2 unit cell) with adsorbed H* have also been computed as a function of H*-coverage and the results are depicted in figure 1. Assuming pairwise additivity in the analysis of DFT data, N–H interactions of 6.2 kcal/mol/ML of H*, at N*-coverage of 0.25, are found. Eventhough such cross interactions can affect the stability of N*, H*, and the energetics of surface reactions, they are weaker in comparison to the strong repulsive N–N interactions. Furthermore, the cross interactions between NH_x–H may also play some role in modifying the stability of NH_x species and changing the energetics of H-abstraction steps due to a high H*–coverage found in our simulations. Future work will address these issues.

4. Development and optimization of surface reaction Mechanism

Ammonia chemistry is modeled with a network of six reversible reactions, shown in table 2, which we treat as elementary. Parameter estimation follows the approach outlined in [37,38]. In brief, the orders of magnitude of the pre-exponential factors are first assigned using transition state theory (TST) [39]. The heats of chemisorption of N and H on a bare surface are obtained from experimental data reported in [40] and are slightly modified to better describe TPD data. The N–N interactions are taken from the DFT calculations with minor modifications indicated below. Heats of chemisorption of NH_x species are calculated using the semi-empirical bond order conservation (BOC) theory (also known as unity bond index–quadratic exponential potential (UBI-QEP) theory) [41,42]. Column 2 in table 1 shows the heats of chemisorption used in the

microkinetic model. UBI-QEP is then used to calculate the activation energies using the heats of chemisorption as input and these are not subject to optimization. The temperature dependence of heats of chemisorption is incorporated using statistical mechanics (see table 1 and [43]). The initial estimates of the pre-exponentials in each step of the mechanism are the only parameters optimized to capture the NH_3 decomposition data of [44]. The parameters of the mechanism are thermodynamically consistent at the free energy level at all temperatures in the typical operational range and has been validated against different sets of experimental data.

In this mechanism, we have used the following relationship for the coverage dependent heat of chemisorption of N:

$$Q_N(\theta_N) = 137.0 - 35.0\theta_N \text{ kcal/mol}.$$

The zero coverage limit of 137 kcal/mol and the interactions of 35 kcal/mol/ML are intermediate between the heat of chemisorption range found in [24,35,40] and our DFT calculations and have been chosen to improve the quantitative comparison with the N_2-TPD data of [8] discussed below. Such an input to UBI-QEP results in coverage dependent activation energies for dissociative N_2 adsorption and associative N_2 desorption as well as for the NH* decomposition and its reverse reaction, as indicated in table 2.

An interesting aspect is that the coverage-dependent heat of reaction for the reversible N_2 adsorption–desorption reaction is negative, i.e., exothermic (for example, −48.1 kcal/mol at 300 K) in the zero coverage limit and becomes positive, i.e., endothermic, at N*-coverage of $\theta_N = 0.69$. Therefore N*-coverages higher than 0.69 are not favorable at 300 K. A similar inference was also presented in [21,45]. Experimentally, sufficient exothermicity is expected for dissociative adsorption to occur, providing a possible reason for the observed submonolayer N*-coverage range of 0.2–0.5 [21–23].

A coverage dependent heat of chemisorption has also been used for hydrogen (see caption of table 2 for details). This coverage dependence affects the energetics of reactions 1, 2, and 5–10 listed in table 2. While H–H interactions have been included in the coverage-dependent model predictions shown below, they are not further discussed here because of their small magnitude.

Next, the optimized mechanism for NH_3 decomposition (hereafter, denoted as parameter set A) is employed to model different experimental data, namely the N_2-TPD data of [8] and the NH_3 decomposition data of [44]. The mean field assumption is employed in all models. The same data are also modeled by merely turning off the N–N interactions from set A (this parameter set is hereafter denoted as set A′). Finally, in order to address the issue of uniqueness of kinetic parameters and elucidate the role of interactions on a fair basis, the pre-exponential factors of the microkinetic model have been re-optimized against the NH_3 decomposition data, in the absence of the N–N interactions (hereafter, denoted as parameter set B). The respective parameter sets A and B are listed in table 2.

Hinrichsen *et al.* [10] developed a microkinetic mechanism for NH_3 synthesis on Cs-promoted Ru that is hereafter denoted as parameter set H, and we employ it for NH_3 decomposition and N_2-TPD on Ru just to assess its predictive capabilities. It should be noted that this mechanism does not explicitly include any N–N interactions. However, the activation energy for N_2 desorption in [10] is intermediate between those in our sets A (activation energy at full N*-coverage) and B (N*-coverage-independent activation energy).

5. Effect of the N–N interactions on mechanism predictions

Comparison of parameter sets A, A′, B, and H with the N_2-TPD data is shown in table 3, in terms of the peak temperatures. Predictions using sets A, A′, and B are also shown in figure 2. It is observed that in the presence of the N–N interactions, the peak locations compare fairly well with the experimental data of [8]. In contrast, in the absence of interactions (sets A′ and B), the spectrum does not shift as much with increasing N*-coverage as shown in figure 2. The overall shift in the peak temperature using set A also compares well with the experimental shift, in contrast to sets A′, B, and H (see table 3).

Figure 3 shows the PFR modeling results using parameter sets A, A′, B, and H for NH_3 decomposition. It is observed that sets A, B, and H capture the

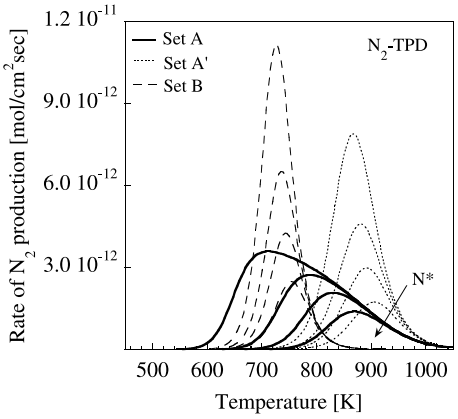

Figure 2. Effect of the N–N interactions on the N_2-TPD. The solid, dotted, and dashed lines correspond to the predictions using parameter sets A, A′, and B, respectively, for four N*-coverages ($\theta_N = 0.25$, 0.15, 0.10, and 0.06 from top to bottom). N–N interactions are essential to capture the magnitude of the shift of the peaks with varying N*-coverage.

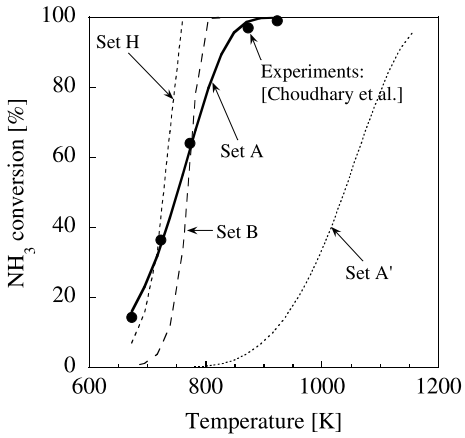

Figure 3. Predictions using various surface reaction mechanisms against experimental data of [44] for NH_3 decomposition. The operating conditions used for modeling the system are: (pure NH_3, pressure = 1 atm, reactor volume = 0.48 cm^3, inlet flow rate = 50 mL/min, number of sites = 6.8×10^{18} sites/g, catalyst weight = 0.1 g). Vastly different pre-exponentials are needed to predict the data well when the N–N interactions are not included. A sharper transition is observed for parameter sets B and H.

data fairly well. In comparison, the predictions of set A′ are poor indicating that the model response is highly sensitive to the N–N interactions. It is possible to capture the experimental features reasonably, without including the N–N interactions (sets B and H) *via*, in our case only pre-exponential factor optimization, but with a completely different set of pre-exponential factors (see table 2). Finally, our modeling demonstrates that there is not a unique set of parameters that can adequately describe the experimental data (albeit the quality of fits of sets A and B is not the same for this specific example). This situation is of course common in kinetics and underlines the inherent uncertainties of the parameters of microkinetic models. Given the large difference in the goodness of fit using sets A and B, inclusion of strong N–N interactions in microkinetic models is essential.

6. Mari analysis

The coverages of the major surface species are plotted in figure 4 for NH_3 decomposition, using the relevant parameter sets at the conditions of figure 3. In the absence of the N–N interactions, N* is the MARI at least at relatively low temperatures, in agreement with most previously published modeling studies. At higher temperatures, the coverage of N* decreases whereas those of * and H* increase. However, the identity of the MARI depends on the specific parameter set. Interestingly, the MARI predictions of sets B and H (figure 4) differ significantly despite the conversion results (figure 3) being similar.

We turn now to parameter set A. In the presence of the N–N interactions, H* dominates as shown in figure 4.

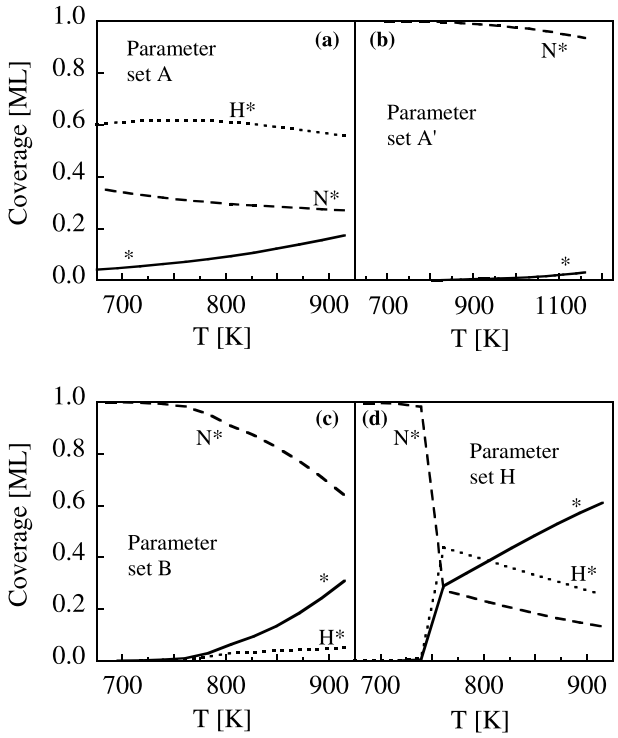

Figure 4. Coverages of major surface species in NH_3 decomposition using the surface reaction parameter sets A (a), A′ (b), B (c), and H (d) for the conditions of figure 3. The N–N interactions alter the MARI. Fast changes in coverages occur with set H at some intermediate temperature.

These predictions are distinctly different from those of all mechanisms that ignore interactions and clearly show that the N–N interactions strongly affect the identity of the MARI. The N*-coverage does not exceed ~0.7 in our predictions when parameter set A is used, a situation that is more consistent with the experimental evidence. In contrast, N*-coverages close to 1.0 are observed with all other sets (A′, B, and H) at sufficiently low temperatures. Finally, figure 4 indicates that no other species are present in high fraction and thus, one can ignore NH_x–NH_x adsorbate–adsorbate interactions.

7. Rate determining step analysis

In order to delineate the role of the N–N interactions in the RDS, sensitivity analysis (SA) has been carried out for NH_3 decomposition (figure 5), where parameter sets A and B are compared. Due to the sharp change in model response of NH_3 conversion, the SA is shown for an intermediate temperature where the NH_3 conversion is approximately 50%.

In the SA carried out here, the pre-exponential factors of both the forward and the backward reactions are perturbed simultaneously. As compared to the conventional perturbation of one step at a time, this approach ensures that the partial equilibrium condition of reversible reactions is not altered and the equilibrium

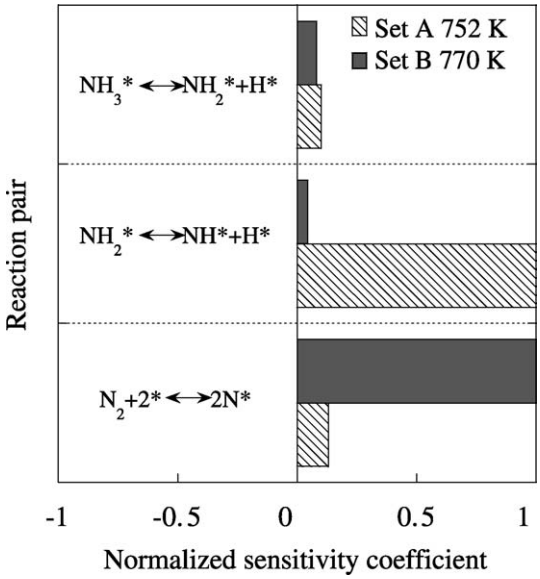

Figure 5. Normalized sensitivity coefficients for parameter sets A and B for NH_3 decomposition. In the absence of the N–N interactions, N_2 desorption is the most important step controlling the NH_3 conversion, whereas in the presence of interactions, NH_2* decomposition is the RDS. This SA is performed at a temperature corresponding to approximately 50% NH_3 conversion.

constant remains fixed, i.e., this SA does not violate the thermodynamics (for a comparison of results to single parameter perturbation and partial equilibrium analysis, see [15]). figure 5 shows such pairwise-perturbation-based SA. A positive normalized sensitivity coefficient implies that a decrease in the pre-exponential factors results in a decrease in the model response, and vice versa.

In the absence of the N–N interactions, N_2 desorption is the most important step, as shown in figure 5, due to the strong blocking of surface sites. The same analysis for set H indicates a similar behavior (not shown). This result is consistent with the previously published hypothesis. On the other hand, in the presence of interactions, N_2 desorbs more readily and the RDS is actually the NH_2* decomposition step (NH_2* + * → NH* + H*). This is because NH_2* decomposition reaction is not in partial equilibrium and exhibits a low net reaction rate due to its high activation energy and low coverage of NH_2* (the NH_2*–coverage is of the order of 10^{-5}–10^{-8}). N_2 desorption plays only a slight role.

Our simulations indicate that the RDS in NH_3 decomposition changes drastically due to the N–N interactions. The repulsive N–N interactions decrease the heat of nitrogen chemisorption along with the activation energy for N_2 desorption, as the N*-coverage increases. This gives rise to easier N_2 desorption and changes the activation energy of NH* decomposition. As a result, some of the surface reaction steps become kinetically significant.

8. Comparison of mechanism energetics with literature values

It is apparent that the reaction energetics and their dependence on adsorbate–adsorbate interactions strongly affect the RDS and the MARI. In order to assess the uncertainty of conclusions, we have compared our energetics with literature values. Periodic slab DFT calculations were carried out by Zhang *et al.* [35] to determine the heats of chemisorption of various species in the NH_3 chemistry and the activation energies of stepwise H-addition reactions on Ru(0001). The coverages employed in these calculations were $\theta_N = \theta_{NH_x} = \theta_H = 0.17$ (a unit cell of 3×2) for the H-addition reactions. Similar DFT calculations were also performed by Logadottir and Norskov [27] on Ru terraces (a unit cell of 2×2) and step sites (a unit cell of 4×2). The coverages in these calculations were $\theta_N = \theta_{NH_x} = \theta_H = 0.25$ for H-addition reactions on terraces, $\theta_N = \theta_H = 0.5$ for N_2 and H_2-adsorption on terraces, $\theta_N = \theta_{NH_x} = \theta_H = 0.125$ for H-addition reactions on step sites, and $\theta_N = \theta_H = 0.25$ for N_2 and H_2-adsorption on step sites. Tables 1 and 4 compare the heats of chemisorption and activation energies, respectively, reported in literature DFT calculations, computed using the semi–empirical UBI–QEP method at two coverage limits ($\theta_N = 0$ and $\theta_N = 0.7$), and from surface science experiments, whenever available. DFT based heats of chemisorption from our work, at quarter monolayer coverage (a unit cell of 2×2), are also included in Table 1.

The heats of chemisorption of N*, H*, and NH_3* are in reasonable agreement with DFT data shown in table 1. On the other hand, heats of chemisorption of the rest NH_x* species predicted by the UBI–QEP method are lower than those predicted by DFT. For some reactions, the activation energies reported using different DFT calculations on terraces differ significantly. As an example for NH_3* decomposition, this difference is 9 kcal/mol. H_2 dissociation is another example. Furthermore, the interesting work of Norskov and coworkers indicates significant differences in energetics between terraces and steps using the same DFT type of simulations. Overall, the agreement between the UBI-QEP method and DFT calculations on step sites is better than on terraces. For example, the activation energy for N_2 dissociative adsorption using DFT was found to be 44.4 kcal/mol on terraces and 9.2 kcal/mol on step sites compared to the experimental value of 7.9 kcal/mole and the UBI-QEP method value that varies from 4.7 to 23.1 kcal/mol as a function of N* coverage. Similar remarks are true for the energetics of associative desorption of N_2. Thus, the UBI-QEP based energetics of N_2 desorption and dissociative adsorption resembles defect sites closer than terrace sites. Given the strong effect of interactions on chemistry predicted by the UBI-QEP method,

Table 1
Comparison of the heats of chemisorption ($Q_{mechanism}$) at zero coverage used in our microkinetic model with those reported in the literature ($Q_{literature}$) or from our DFT

Species	$Q_{mechanism}$ (kcal/mol)	$Q_{literature}$ (kcal/mol)	Temperature dependence [a] $\frac{Q(T_0 - Q(T)}{R\Delta T}$	Changes in degrees of freedom to derive the temperature dependence [b]
H	64.0	62.4[c] [47] 62.3[c] [48] 63.0 [40] 68.7[d] [35] 58.0[d] [27] 58.3[e] [27] 65.0[d] (this work)	1.5	−3T + 3V
N	137.0	135.0 [40] 140.8[d][24] 131.4[d][35] 119.6[d][27] 122.2[e][27] 128.2[d] (this work)	1.5	−3T + 3V
NH	86.6	87.0[f] [40] 111.8[d] [35] 99.6[d] [27] 100.3[e][27] 105.4[d] (this work)	2.0	−3T − 2R + RR + 4V
NH_2	60.9	60.0[f] [40] 68.0[d] [35] 46.6[d] [27] 70.9[e] [27] 66.7[d] (this work)	2.5	−3T − 3R + RR + 5V
NH_3	20.0	25.1[g] [16] 18.0[f] [40] 20.5[d] [35] 9.5[d] [27] 20.0[e] [27] 24.8[d] (this work)	2.5	−3T − 3R + RR + 5V

The latter values are provided only for comparison. The values for NH_x species in the second column are computed using the UBI-QEP method. The literature values come from surface science experiments, the semi-empirical UBI-QEP theory, or DFT calculations. The DFT calculations of [35] are at coverages of $\theta_N = \theta_{NH_x} = \theta_H = 0.17$ (a unit cell of 3×2) whereas our DFT calculations are at a quarter monolayer coverage (a unit cell of 2×2). The coverages in the DFT calculations of [27] on terraces and step sites are $\theta_N = \theta_{NH_x} = \theta_H = 0.25$ (a unit cell of 2×2) and $\theta_N = \theta_{NH_x} = \theta_H = 0.125$ (a unit cell of 4×2), respectively. The zero point energy correction is not accounted for in either [27] or our DFT calculations. The last two columns indicate the temperature dependence of the heats of chemisorption based on statistical mechanics [43]. The heat of chemisorption, $Q(T)$, decreases with increasing temperature (here $\Delta T = T - T_0$ and $T_0 = 300$ K).

[a]The general assumptions invoked in calculating the temperature dependence are as follows: (1) Each translational, rotational, and vibrational degree of freedom (DOF) accounts for 0.5RT, 0.5RT, and RT, respectively. (2) All translational DOF are converted into vibrational DOF upon adsorption. (3) Upon adsorption, all rotational DOF are converted into vibrational DOF. For species with a vertical axis through the adsorbed atom, such as NH*, NH_2*, and NH_3*, 1 of the gained vibrational DOF is assumed to be a free, internal rotor (rigid rotor approximation) and counts as 0.5RT.

[b]T, R, and V denote translational, rotational, and vibrational DOF. RR implies that a vibrational DOF is considered to be a free, internal rotor. The 'minus' and 'plus' signs indicate loss and gain of DOF, respectively.

[c]Calculated from the reported experimental H_2 desorption energy.

[d]DFT on terraces.

[e]DFT on step sites

[f]Predicted using the UBI–QEP method.

[g]Obtained from TPD fitting.

Table 2
Reaction steps and associated parameters for NH_3 decomposition on supported Ru for parameter sets A (first row of parameters for each reaction) and B (second row of parameters for each reaction) at a typical temperature of 773 K

Reaction no.	Reaction	Sticking coefficient (unitless) or pre-exponential factor (s^{-1})	Activation energy (kcal/mol)
1	$H_2 + 2* \rightarrow 2H*$	8.7×10^{-1}	0.0
		7.0×10^{-2}	0.0
2	$2H* \rightarrow H_2 + 2*$	1.1×10^{11}	$19.6-7.0\theta_H$
		2.5×10^{13}	$19.6-7.0\theta_H$
3	$N_2 + 2*$ $2N*$	2.0×10^{-1}	$7.1 + 26.3\theta_N$
		6.3×10^{-3}	7.1
4	$2N* \rightarrow N_2 + 2*$	1.7×10^{12}	$51.0-43.8\theta_N$
		1.0×10^{15}	51.0
5	$NH* + * \rightarrow N* + H*$	1.9×10^{12}	$5.3 + 15.5\theta_N + \theta_H$
		3.6×10^{9}	$5.3 + \theta_H$
6	$N* + H* \rightarrow NH* + *$	7.6×10^{9}	$37.6 - 19.5\theta_N - 2.5\theta_H$
		1.6×10^{12}	$37.6 - 2.5\theta_H$
7	$NH_2* + * \rightarrow NH* + H*$	2.0×10^{12}	$20.1 + 1.2\theta_H$
		4.5×10^{12}	$20.1 + 1.2\theta_H$
8	$NH* + H^* \rightarrow NH_2* + *$	1.4×10^{10}	$15.9-2.3\theta_H$
		2.0×10^{12}	$15.9-2.3\theta_H$
9	$NH_3* + * \rightarrow NH_2* + H*$	2.0×10^{12}	$18.7 + 1.3\theta_H$
		2.0×10^{11}	$18.7 + 1.3\theta_H$
10	$NH_2* + H* \rightarrow NH_3* + *$	3.4×10^{9}	$11.6 - 2.2\theta_H$
		1.8×10^{10}	$11.6 - 2.2\theta_H$
11	$NH_3 + * \rightarrow NH_3*$	1.5×10^{-4}	0.0
		1.1×10^{-3}	0.0
12	$NH_3* \rightarrow NH_3 + *$	8.1×10^{11}	17.7
		2.4×10^{11}	17.7

the substantial differences between DFT simulations in table 4 on terrace sites may in part be due to the different coverages invoked.

Differences in energetics between the UBI-QEP method and DFT calculations for the H-addition and abstraction reactions are also observed. Regarding the predicted RDS of NH_2* decomposition, the activation energy of the microkinetic model is in between the DFT numbers on terraces and step sites. Given the disparity between DFT numbers and in particular, the role of defects elucidated by DFT, the difference between the UBI-QEP method and DFT numbers, and the strong effect of interactions elucidated herein, we believe that the RDS and the MARI in NH_3 decomposition may depend on the method used for the calculation of energetics. This comparison highlights again the multi-scale nature of catalytic processes discussed above that

Table 3
Effect of N–N interactions on the N_2–TPD peak temperatures against experimental data of Dahl *et al.* [8]

N*-coverage	Peak temperature				
	(Expts.) (K)	(Set A) (K)	(Set A′) (K)	(Set B) (K)	(Set H) (K)
0.25	689	712	868	727	659
0.15	764	788	879	735	672
0.10	783	830	891	743	682
0.06	840	868	906	754	696
Net change in N*-coverage	Net change in peak temperature				
	(Expts.) (°C)	(Set A) (°C)	(Set A′) (°C)	(Set B) (°C)	(Set H) (°C)
0.19	151	156	38	27	37

Peak temperatures using parameter sets A, A', B, and H are reported for four N*-coverages (θ_N = 0.25, 0.15, 0.10, and 0.06). N–N interactions are essential to capture the magnitude of the shift in the peaks with varying N*-coverage. The net change in the peak temperature is also shown for the overall N*-coverage range.

makes truly first principles predictions for catalysts of practical interest difficult.

9. Conclusions

Adsorbate–adsorbate interactions between N atoms on Ru(0001) were estimated using periodic slab DFT calculations and incorporated in a microkinetic model for NH_3 decomposition at atmospheric pressure and N_2-TPD at UHV conditions. Similar DFT simulations indicate that N–H interactions are much weaker than N–N interactions. Based on the results of the microkinetic model with UBI-QEP predicted activation energies, the RDS in NH_3 decomposition is the N–H bond cleavage in NH_2*, whereas the associative desorption of nitrogen contributes to the overall rate to a much less extent. Under typical decomposition conditions, H* followed by N* are the MARI. Overall, our analysis shows that N–N interactions considerably alter the identity of the MARI and the RDS in NH_3 decomposition chemistry, giving rise to different conclusions about the kinetically significant steps from most previously published work. While fixed bed reactor decomposition data can be adequately described using mechanisms that lack adsorbate–adsorbate interactions, the latter are essential to capture the N_2-TPD data, the submonolayer saturation N*-coverage, and the physics of the important NH_3/Ru chemistry.

Acknowledgments

This work was supported by the Army Research Office under contract DAAD19-01-1-0582. Any opin-

Table 4
Comparison of activation energies at two coverages from our model at 300 K computed using the UBI-QEP with those reported in the literature

Reaction	E_f(kcal/mol)	E_b(kcal/mol)
$H_2 + 2* \leftrightarrow 2H*$	0.0[a,b]	23.8[a,b]
	0.0[c] [35]	33.2[c] [35]
	0.0[c] [27]	11.8[c] [27]
	0.0[d]	12.3[d] [27]
	0.0[c] (this work)	25.6[c,e] (this work)
$N_2 + 2* \leftrightarrow 2N*$	4.7[a]	52.8[a]
	23.1[b]	22.2[b]
	7.9[f][46]	44.2[f] [46]
	44.4[c] [27]	57.7[c] [27]
	9.2[d] [27]	27.7[d] [27]
$NH* + * \leftrightarrow N* + H*$	4.5[a]	39.1[a]
	15.3[b]	25.5[b]
	27.0[c] [35]	26.1[c] [35]
	30.1[c] [27]	28.3[c] [27]
	24.7[d] [27]	25.1[d] [27]
$NH_2* + * \leftrightarrow NH* + H*$	19.3[a,b]	17.5[a,b]
	16.4[c] [35]	29.5[c] [35]
	10.2[c] [27]	29.7[c] [27]
	34.8[d] [27]	31.0[d] [27]
$NH_3* + * \leftrightarrow NH_2* + H*$	17.6[a,b]	13.6[a,b]
	29.3[c] [35]	27.7[c] [35]
	38.2[c] [27]	32.5[c] [27]
	20.5[d] [27]	29.5[d] [27]
$NH_3 + * \leftrightarrow NH_3*$	0.0[a,b]	20.0[a,b]
	0.0[c] [35]	20.5[c] [35]
	0.0[c] [27]	9.5[c] [27]
	0.0[d] [27]	20.0[d] [27]
	0.0[c] (this work)	24.8[c] (this work)

The H*-coverage dependence is left out in this comparison. E_f and E_b represent the forward and backward activation energies, respectively. The literature DFT values are at coverages of $\theta_N = \theta_{NH_x} = \theta_H = 0.17$ (H-addition reactions) [35], $\theta_N = \theta_{NH_x} = \theta_H = 0.25$ (H-addition reactions on terraces) and $\theta_N = \theta_H = 0.5$ (N_2 and H_2-adsorption on terraces) [27], and $\theta_N = \theta_{NH_x} = \theta_H = 0.125$ (H-addition reactions on step sites) and $\theta_N = \theta_H = 0.25$ (N_2 and H_2-adsorption on step sites) [27]. Zero point energy correction is not accounted for in [27]. For H_2 desorption, the activation energy is calculated using the heat of chemisorption of H, so that enthalpic consistency is maintained, whereas for NH_3* desorption, the activation energy is equal to the heat of chemisorption of NH_3. The values reported here are merely for comparison purposes at a particular coverage as they are computed automatically in our simulations.
[a]Calculated at $\theta_N = 0$ using UBI-QEP.
[b]Calculated at $\theta_N = 0.7$ using UBI-QEP.
[c]DFT on terraces.
[d]DFT on step sites.
[e]E_b is calculated using thermodynamic balance.
[f]HREELS and TPD experiments.

ions, findings, and conclusions or recommendations expressed are those of the authors and do not necessarily reflect the views of the Army Research Office.

References

[1] J. C. Ganley, E. G. Seebauer and R. I. Masel, AIChE J. 50 (2004) 829.
[2] F. Haber and G. van Oordt, Z. Anorg. Chem. 43 (1904) 111.
[3] F. Haber and G. van Oordt, Z. Anorg. Chem. 44 (1905) 341.
[4] W. Tsai and W. H. Weinberg, J. Phys. Chem. 91 (1987) 5302.
[5] S. Dahl, P. A. Taylor, E. Tornquist and I. Chorkendorff, J. Catal. 178 (1998) 679.
[6] C. J .H. Jacobsen, S. Dahl, B. S. Clausen, S. Bahn, A. Logadottir and J. K. Norskov, J. Am. Chem. Soc. 123 (2001) 8404.
[7] J. C. Ganley, E. G. Seebauer and R. I. Masel, (2003) in preparation.
[8] S. Dahl, E. Tornquist and I. Chorkendorff, J. Catal. 192 (2000) 381.
[9] O. Hinrichsen, F. Rosowski, A. Hornung, M. Muhler and G. Ertl, J. Catal. 165 (1997) 33.
[10] O. Hinrichsen, F. Rosowski, M. Muhler and G. Ertl, Stud. Surf. Sci. Catal. 109 (1997) 389.
[11] L. Diekhoner, H. Mortensen, A. Baurichter and A. C. Luntz, J. Vac. Sci. Tech. A 18 (2000) 1509.
[12] L. Diekhoner, H. Mortensen, A. Baurichter and A. C. Luntz, J. Chem. Phys. 115 (2001) 3356.
[13] S. Dahl, A. Logadottir, C. J. H. Jacobsen and J. K. Norskov, Appl. Catal. A: Gen. 222 (2001) 19.
[14] M. C. J. Bradford, P. E. Fanning and M. A. Vannice, J. Catal. 172 (1997) 479.
[15] S. R. Deshmukh, A. B. Mhadeshwar and D. G. Vlachos, Ind. Eng. Chem. Res. (2003) in press.
[16] S. Dahl, J. Sehested, C. J. H. Jacobsen, E. Tornquist and I. Chorkendorff, J. Catal. 192 (2000) 391.
[17] L. Diekhoner, A. Baurichter, H. Mortensen and A. C. Luntz, J. Chem. Phys. 112 (2000) 2507.
[18] M. Boudart and G. Djega–Mariadassou, Kinetics of Heterogeneous Catalytic Reactions (Princeton University Press, Princeton, 1984).
[19] H. Dietrich, K. Jacobi and G. Ertl, Surf. Sci. 352 (1996) 138.
[20] H. Dietrich, K. Jacobi and G. Ertl, J. Chem. Phys. 106 (1997) 9313.
[21] S. Schwegmann, A. P. Seitsonen, H. Dietrich, H. Bludau, H. Over, K. Jacobi and G. Ertl, Chem. Phys. Lett. 264 (1997) 680.
[22] H. Dietrich, K. Jacobi and G. Ertl, J. Chem. Phys. 105 (1996) 8944.
[23] H. Rauscher, K. L. Kostov and D. Menzel, Chem. Phys. 177 (1993) 473.
[24] K. Jacobi, Phys. Stat. Sol. A 177 (2000) 37.
[25] B. Hammer, Phys. Rev. B 63 (2001) 205423(1).
[26] J. J. Mortensen, Y. Morikawa, B. Hammer and J. K. Norskov, J. Catal. 169 (1997) 85.
[27] A. Logadottir and J. K. Norskov, J. Catal. 220 (2003) 273.
[28] I. Alstrup, I. Chorkendorff and S. Ullmann, J. Catal. 168 (1997) 217.
[29] H. Dietrich, P. Geng, K. Jacobi and G. Ertl, J. Chem. Phys. 104 (1996) 375.
[30] G. Ertl, Heterogeneous catalysis on the atomic scale. in: *The Chemical Record*, Vol. 1 (The Japan Chemical Journal Forum and John Wiley & Sons, NewYork, 2000) p. 33.
[31] P. Stoltze and J. K. Norskov, Phys. Rev. Lett. 55 (1985) 2502.
[32] S. R. Deshmukh, A. B. Mhadeshwar, M. Lebedeva and D. G. Vlachos, Int. J. Multiscale Comp. Eng. (2004) accepted.
[33] D. Vanderbilt, Phys. Rev. B 41 (1990) 7892.
[34] B. Hammer, O. H. Nielsen, J. J. Mortensen, L. Bengtsson, L. B. Hansen, A. C. E. Madsen, Y. Morikawa, T. Bligaard and A. Christensen, DACAPO *version 2.7* (CAMP, Technical University, Denmark).
[35] C. J. Zhang, M. Lynch and P. Hu, Surf. Sci. 496 (2002) 221.
[36] D. J. Dooling, R. J. Nielsen and L. J. Broadbelt, Chem. Eng. Sci. 54 (1999) 3399.
[37] Y. K. Park, P. Aghalayam and D. G. Vlachos, J. Phys. Chem. A 103 (1999) 8101.
[38] P. Aghalayam, Y. K. Park and D. G. Vlachos, AIChE J. 46 (2000) 2017.

[39] J. A. Dumesic, D. F. Rudd, L. M. Aparicio, J. E. Rekoske and A. A. Trevino, The Microkinetics of Heterogeneous Catalysis (American Chemical Society, Washington, DC, 1993).
[40] E. Shustorovich and A. T. Bell, Surf. Sci. Lett. 259 (1991) L791.
[41] E. Shustorovich and H. Sellers, Surf. Sci. Rep. 31 (1998) 1.
[42] E. Shustorovich, Adv. Catal. 37 (1990) 101.
[43] A. B. Mhadeshwar, H. Wang and D. G. Vlachos, J. Phys. Chem. B 107 (2003) 12721.
[44] T. V. Choudhary, C. Sivadinarayana and D. W. Goodman, Catl. Lett. 72 (2001) 197.
[45] L. Diekhoner, H. Mortensen, A. Baurichter, A. C. Luntz and B. Hammer, Phys. Rev. Lett. 84 (2000) 4906.
[46] H. Shi, K. Jacobi and G. Ertl, J. Chem. Phys. 99 (1993) 9248.
[47] G. Lauth, E. Schwarz and K. Christmann, J. Chem. Phys. 91 (1989) 3729.
[48] N. Savargaonkar, R. L. Narayan, M. Pruski, D. O. Uner and T. S. King, J. Catal. 178 (1998) 26.
[49] R. L. Narayan and T. S. King, Thermochim. Acta 312 (1998) 105.